Published in final edited form as:
J Am Soc Mass Spectrom. 2014 April ; 25(4): 563–571. doi:10.1007/s13361-013-0815-6.

Implementation of Dipolar Resonant Excitation for Collision Induced Dissociation with Ion Mobility/Time-of-Flight MS

Ian K. Webb, **Tsung-Chi Chen**, **William F. Danielson III**, **Yehia M. Ibrahim**, **Keqi Tang**, **Gordon A. Anderson**, and **Richard D. Smith***
Biological Sciences Division and Environmental Molecular Sciences Laboratory, Pacific Northwest National Laboratory, 3335 Innovation Ave. (K8-98), P.O. Box 999, Richland, Washington, USA 99352

Abstract

An ion mobility/time-of-flight mass spectrometer (IMS/TOF MS) platform that allows for resonant excitation collision induced dissociation (CID) is presented. Highly efficient, mass-resolved fragmentation without additional excitation of product ions was accomplished and over-fragmentation common in beam-type CID experiments was alleviated. A quadrupole ion guide was modified to apply a dipolar AC signal across a pair of rods for resonant excitation. The method was characterized with singly protonated methionine enkephalin and triply protonated peptide angiotensin I, yielding maximum CID efficiencies of 44% and 84%, respectively. The Mathieu $q_{x,y}$ parameter was set at 0.707 for these experiments to maximize pseudopotential well depths and CID efficiencies. Resonant excitation CID was compared to beam-type CID for the peptide mixture. The ability to apply resonant waveforms in mobility-resolved windows is demonstrated with a peptide mixture yielding fragmentation over a range of mass-to-charge (*m/z*) ratios within a single IMS-MS analysis.

Keywords

Ion mobility spectrometry; Collision induced dissociation; Peptide dissociation

Introduction

Collision induced dissociation (CID), the “gold standard” of ion fragmentation in mass spectrometry (MS), has been universally applied to a range of analytical chemistry applications due to its efficiency, ease of implementation, and instrument control [1]. In the CID process, ions are electronically and/or vibrationally excited through energetic collisions with an inert neutral target gas [2]. Multiple MS platforms have been employed for structural analysis by CID, including sector [3], triple quadrupole [4], quadrupole ion trap [5], quadrupole time-of-flight (qTOF) [6], time-of-flight/time-of-flight (TOF/TOF) [7], and Fourier transform-ion cyclotron resonance (FT-ICR) [8] instruments. The implementation of CID generally falls into one of two approaches: i.) axial excitation or ii.) radial excitation. CID via axial excitation is accomplished by accelerating ions along the axis of a beam

*Corresponding Author. rds@pnnl.gov.

geometry instrument into a collision cell containing the target gas [2]. This is typically accomplished by establishing a DC potential gradient through the acceleration region and is amenable to sector, triple quadrupole, qTOF, or TOF/TOF instruments. The advantages of this method include the wide range of energies available with different instrument geometries (eV-keV) and ease of implementation (viz. increasing a DC bias voltage) [3–4, 6–7]. Radial excitation by RF heating is implemented by displacing ions close to a RF multipole ion guide or ion trapping instrument, increasing the amplitude of ion micromotion by energy absorption from the RF field [9]. RF heating can be implemented in a broadband fashion by using DC potentials [10–14] or low frequency AC [15] in the radial axis or in a mass selective fashion by applying a dipolar waveform in resonance with the fundamental secular frequency of ion motion in the RF multipole ion guide[16–17]. Dipolar AC resonant excitation CID enjoys the advantage of only exciting ions over a limited mass-to-charge (*m/z*) ratio range without need for precursor ion isolation as the secular frequency is *m/z* dependent. In addition, product ions are generally no longer in resonance with the excitation signal, effectively eliminating over-fragmentation while also allowing very high efficiency.

Over the past several decades, “low energy” (<100 eV translational energy) CID has been applied extensively to structural studies of biologically-relevant macromolecules owing to broad effectiveness and applicability of “soft” ionization methods [18–19]. An important application of low energy CID is to peptide identification using tandem MS analysis (MS/MS) [20]. The tandem MS/MS technique, often coupled with a reversed-phase liquid chromatography (RPLC) separation, has been effectively applied to “bottom-up” proteomics in which proteins are enzymatically digested and identified by the sequence identification of all the substituent peptides [21]. There are challenges with the “bottom-up” approach. The first challenge is coelution of peptides. Complex mixtures contain a multitude of peptides, leading to complex mass spectra even after LC separation. The second challenge arises from the first. The traditional “bottom-up” approach utilizes tandem MS for peptide identification, but the selection of single peptides for tandem MS analysis suffers from low duty cycles, as peptides that coelute with the chosen peptide are not analyzed. The result is limited coverage of digested proteins, leading to far less peptide and protein identifications. Multiplexed MS/MS methods have been developed that allow for fragmentation of all coeluting peptide ions throughout the “bottom-up” experiment to increase ion utilization duty cycles [22–27]. However, there are fundamental difficulties in the implementation of multiplexed methods as well. The product ions of coeluting peptides are convoluted, making it difficult to assign the fragment ions to their corresponding peptides. Another inherent issue with multiplexed methods is the choice of a collision energy that is effective for the fragmentation of all the coeluting peptides, as over or under-fragmentation of peptide ions can result in a loss of sequence information and instrument sensitivity for the identification [28].

Ion mobility/collision induced dissociation/mass spectrometry (IMS/CID/MS) approaches have been developed for peptide fragmentation and are particularly well suited to combat the deficiencies of multiplexed MS/MS methods. IMS relies upon the effects of the collisional cross sections of ions, travelling via an electric field in a drift cell containing a background gas, upon their velocities [29–32]. IMS can be performed in a lossless fashion, allowing for greater proteomic coverage by reducing the complexity of mass spectra, owing to

orthogonality of IMS to LC and MS analyses [33–39]. By fragmenting ions after IM separation, both precursor and product ions have essentially the same drift times, allowing for product ions to be matched to their corresponding precursors [40] to increase the number of peptide identifications. In addition, the over and under-fragmentation problems have been somewhat alleviated by matching different CID energies to different drift times [41]. The optimal CID energy has been shown to be linearly related to drift time in previous studies that employed ramping the CID energy with increasing drift times [42]. Unfortunately, initial attempts at variable collision energy IMS/CID/MS yielded low fragmentation efficiencies (~30% for multiply charged ions of bovine serum albumin) [42]. The implementation of a segmented quadrupole operated at 200 mTorr helped increase efficiency, but in that implementation, CID energies were not related to ion drift times [43], not allowing for efficient fragmentation for complex mixtures covering a broad *m/z* range. Thus, the ability to relate CID energy with drift time while maintaining high fragmentation efficiency is desired.

The current implementation of multiplexed IMS/CID/MS utilizes variable energy dipolar AC resonant excitation CID in a quadrupole ion guide after IM separation of ions for mass and mobility-resolved excitation with high efficiency. The benefits of the approach includes the ability to apply drift time resolved CID energies over an *m/z* range that is relevant to bottom-up proteomics measurements (e.g. *m/z* ~300–1200). In addition peptides are fragmented without the need for precursor ion isolation, greatly improving duty cycle, and the fragmentation is done in a fashion mitigating over-fragmentation due to further excitation of fragment ions. The purpose of this study is to explore the efficiency of dipolar resonant excitation applied in mobility-resolved windows for model peptides and to evaluate fragmentation using a mixture of peptide ions.

Experimental

Methods

Experiments were performed on a home-built nanoelectrospray (nanoESI)-IMS-QTOF MS instrument that has been described previously in the literature (Fig. 1) [43]. Briefly, ions are formed in the nanoESI source by 300 nL/min direct infusion at an applied potential of 4.3 kV. The source and drift tube regions of the instrument are floated to 1.8 kV. Ions are sampled by a stainless steel heated capillary operated at 120 °C into a dual-ion funnel interface [44–46]. The first ion funnel is operated at 12 Torr and is offset by a few mm from the entrance aperture of the second funnel, an ion funnel trap operated at 3.95 Torr [47–48]. The ions are trapped for ~5 ms and pulsed out of the trap for ~0.5 ms. The drift tube is operated at 4 Torr N_2 with an electric field of 17 V/cm. Maintaining a slightly positive pressure of 50 mTorr between the IMS drift cell and the ion funnel trap helps to minimize gas dynamics effects and prevent neutrals from entering the drift tube. Ions are sampled at the end of the drift tube by a third ion funnel and focused into the exit optics; viz. a short quadrupole, operated at a driving RF frequency of 1.3 MHz and amplitude of 125 $V_{p\text{-}p}$, and a collision quadrupole, operated at variable RF frequencies and amplitudes. Pressure in the short quadrupole was kept at ~400 mTorr and the collision quadrupole was operated at ~80 mTorr. Both quadrupoles had inscribed radii of r_0 = 2.8 mm. The collision cell utilized vane

electrodes running longitudally along the quadrupole between each pair of rods to allow for a DC potential gradient to be established in the axial direction to avoid broadening the arrival time distribution through the collision cell (Fig. 2(a)). A DC gradient of 35 V was used between the last electrode of the rear ion funnel and the exit orifice plate after the collision quadrupole. Each of the four vane electrodes was divided into 6 segments, each 11.58 mm long, spaced by 0.51 mm between consecutive segments. The first four segments and the final two segments were each resistively coupled, yielding two separate vane sections controlled by four DC power supplies. The home-built portion of the instrument was directly coupled to an Agilent 6538 QTOF MS (Agilent, Santa Clara, CA, USA) utilizing a 1.5 m flight tube. The standard ESI source was removed and collision quadrupole exit plate was mated to the entrance octopole ion guide of the QTOF.

The resonant excitation waveforms were superimposed on the main RF of the collision quadrupole (Fig. 2(b)). One pair of rods received a single phase of RF with the rods electrically coupled, while the other pair contained electrically isolated rods. The waveforms were applied to the primary coil of a toroidal transformer, wound in a turn ratio of 10:40:40 with two secondary coils. The second phase of the drive RF was applied to both secondary coils, and the outputs were wired to the second pair of rods. Waveforms were generated by a NI PXI-5412 arbitrary waveform generator (National Instruments Corporation, Austin, TX, USA). Software written in C# was developed in-house to apply waveforms in variable time windows during each IMS separation to match the arrival times of ions in the collision quadrupole. Waveforms applied were the sums of individual sine waves calculated for the secular frequencies of particular ions of interest. Secular frequencies (ω) were calculated by the following equation for ion motion in a purely quadrupolar RF field

$$\omega = \left(\frac{\beta}{2}\right)\Omega \quad (1)$$

where β refers to the iso-β_r lines from the Mathieu stability diagram and Ω is the frequency of quadrupolar RF. β is calculated from the approximation

$$\beta = \left(\frac{{q_{x,y}}^2}{2}\right)^{\frac{1}{2}} \quad (2)$$

where $q_{x,y}$ represents the Mathieu stability parameter in the radial dimension, given by

$$q_{x,y} = \frac{4eV}{mr_0^2\Omega_0^2} \quad (3)$$

The previous approximation holds for low values of $q_{x,y}$ <0.2 but nevertheless provided secular frequencies that were experimentally validated for inducing fragmentation [17].

Materials

Angiotensin I human acetate salt hydrate, [Met^5]enkephalin acetate salt hydrate, neurotensin, substance P acetate salt hydrate, and melittin from honey bee venom were purchased from Sigma-Aldrich (St. Louis, MO, USA). Solutions of angiotensin I and

methionine enkephalin were used in concentrations of 1 μM. A four peptide mixture solution was made from 1 μM each angiotensin I, neurotensin, substance P, and melittin. Each solution was made in a matrix of 50:50:1 methanol:water:acetic acid and samples were used without further purification.

Results and Discussion

Methionine Enkephalin

The initial characterization of the dipolar AC excitation method was performed utilizing the singly protonated peptide methionine enkephalin (YGGFM, *m/z* 574.2). A dipolar AC resonant excitation waveform of 338 kHz, 8 V_{p-p} was applied across a pair of rods with the main RF set to 1.35 MHz, 1188 V_{p-p}. The dipolar waveform was applied from time 29–34 ms determined by the observed drift time distribution of the precursor methionine enkephalin ion. The CID amplitude, 8 V_{p-p}, is much higher than CID voltages used in typical ion trap CID experiments [17]. Higher amplitudes are necessary due to the much shorter residence times of the ions in the collision quadrupole (~0.1 – 1 ms) than that in ion traps (~10–100 ms). The operating drive main RF amplitude yields a Mathieu $q_{z,y}$ value of 0.707, placing the ion in the deepest pseudopotential well depth[17]. The pseudopotential well depth model gives an estimation of well depth in a quadrupole by the following relation [17]

$$\overline{D}=\frac{1}{4}qV \quad (4)$$

The well depth for methionine enkephalin under the given main RF is 105 eV.

The resonant excitation CID product ion spectrum of methionine enkephalin is shown in Figure 3 (a) as a nested IMS/MS spectrum with drift time as the x-axis, *m/z* as the y-axis, and abundance given by color contours. For comparison, the nested IMS/MS spectrum for methionine enkephalin without the application of dipolar AC is given in Supplemental Figure 1. Figure 3 (a) shows that the fragment ions retain the same drift time as the precursor ion since fragmentation occurs after drift time separation and the flight time of the ions after the drift tube and before arrival at the TOF detector is short (~1.2 ms for the pressures used) compared to drift times (~20–30 ms) [40, 42–43]. The largest shift in drift time observed was 163 μs, between the abundance maxima of the smallest fragment (F immonium ion) and a *m/z* 574.2 precursor. This is comparable to the shift in drift times observed for methionine enkephalin and its products from a previous study [43]. Such shifts occur due to the slight difference in flight times between the smallest and largest ions after dissociation in the collision quadrupole before reaching the TOF detector. The observed fragment ions are annotated in the mass spectrum of the experiment (Fig. 3 (b)). Several observations can be made from the product ion spectrum. First, the a_4 to b_4 abundance ratio favors a_4 (1.5:1), typical for CID of protonated enkephalin ions [49]. The a_4 and b_4 ions are typically the favored dissociation pathways since these fragmentation channels have the smallest activation barriers. Second, the third most abundant ion is b_3, commonly observed since it has the next lowest reaction barrier. Third, the y_2 and y_3 ions are the major C-terminal fragments observed, with a smaller fraction of y_4. Other observed fragments

include y_1, b_2, the C-terminal immonium ion F, the N-terminal immonium ion Y, and the internal fragments GF and GGF. An important feature is the ability to transfer and detect low mass fragments. For example, the calculated $q_{x,y}$ parameter for F (*m/z* 120.1) under the conditions used is 3.38, far beyond the region of stability for transmittable ions through the collision cell ending with a $q_{x,y}$ value of 0.908. The calculated low mass cutoff for the collision cell under the given RF is *m/z* 447.1. Therefore, though the ions gain kinetic energy in the collision cell during dipolar excitation, the short ion residence times in the quadrupole largely delays fragmentation (or loss of fragments) until after exiting the collision cell. The results are similar to pulsed-q dissociation or high-amplitude short-time excitation (HASTE) physically separated in two separate ion guides rather than temporally separated within an ion trap [50–52], which excite ions in a ~100 μs to a few ms timescale. The observed sequence ions provide 100% sequence coverage of methionine enkephalin.

Fragmentation (E_f), collection (E_c), and CID (E_{CID}) efficiencies were measured for dipolar excitation CID of methionine enkephalin (Table 1 (a)) as additional figures of merit. These quantities are calculated in the following fashion [53–54]:

$$E_f = \frac{\Sigma f}{P + \Sigma f} \quad (5)$$

$$E_c = \frac{P + \Sigma f}{P_0} \quad (6)$$

$$E_{CID} = \frac{\Sigma f}{P_0} = (E_f)(E_c) \quad (7)$$

P_0 refers to the initial abundance of precursor ion, P is the remaining precursor ion abundance after fragmentation, and Σf is the sum of the fragment ion abundances. The data in Table 1 show the effects of the applied dipolar excitation amplitude on efficiency. Amplitudes below 7.2 $V_{p\text{-}p}$ have the highest collection efficiencies, but much lower fragmentation efficiencies. This is due to under-fragmentation as a result of many ions not reaching high enough internal energies to fragment with the amplitudes used. The CID efficiency is highest at 7.2 $V_{p\text{-}p}$ at 44%, which compares favorably to triple quadrupole and other beam CID experiments on singly charged peptide ions[43]. Increasing the CID amplitude above 7.2 $V_{p\text{-}p}$ does give higher fragmentation efficiencies but at the cost of significantly lower collection efficiencies. One explanation for the observed reduction in collection efficiency at higher amplitudes is resonant ejection of the precursor ions. However, the fragmentation efficiency decreases at the highest CID amplitude, corresponding to product ion loss either due to low mass cutoff issues or losses at the exit aperture of the collision cell or entrance to the octopole. The former explanation is not likely as the low mass cutoff remains constant throughout the experiment and the (a_4 + b_4) to (F + Y) intensity ratios actually decreases from activation amplitudes of 8.8 $V_{p\text{-}p}$ to 9.6 $V_{p\text{-}p}$, with ratios of 5.41:1 for 8.8 $V_{p\text{-}p}$ and 2.406:1 for 9.6 $V_{p\text{-}p}$, respectively. (Supplemental Fig. 2).

Angiotensin I

The nested IMS/MS product ion spectrum of the $[M + 3H]^{3+}$ charge state of angiotensin I is shown in Figure 4 (a). Angiotensin I ($[M + 3H]^{3+}$) was used as a model multiply charged peptide ion. The Mathieu $q_{x,y}$ parameter was set to 0.707 by utilizing a main RF of 1.35 MHz and an amplitude of 895 V_{p-p}. The precursor ion IMS/MS spectrum is given in Supplemental Figure 3. CID was performed by applying a 336 kHz, 8.8 V_{p-p} waveform from drift time 21 to 26 ms. The largest deviation in drift time is 488 μs, between the maxima of the $[M+3H]^{3+}$ (*m/z* 432.9) precursor ion and b_9^{2+} (*m/z* 583.3) product ion. The fragment ion peaks from the IMS/CID/MS experiment are labeled in the mass spectrum in Figure 4 (b). The most dominant dissociation pathway is cleavage N-terminal to the proline residue yielding the y_4/b_6^{2+} and y_4^{2+}/b_6 fragment ion pairs as is expected from the so-called "proline effect" [55–60]. Combined with the other observed a, b, and y fragments, ~55% sequence coverage is achieved. The fragmentation, collection, and CID efficiencies were tabulated in Table 1 (b) as a function of excitation amplitude. Fragmentation efficiencies increase as excitation amplitudes increase until all precursor is depleted at 8.8 V_{p-p}. The collection efficiencies remain similar until they start to decrease dramatically at 8.8 V_{p-p}. These two observations point to the loss of precursor before 8.8 V_{p-p} is reached by resonant ejection instead of fragmentation. The highest CID efficiency observed was 84% using an excitation amplitude of 8.32 V_{p-p}, beyond which point resonant ejection of the precursor begins to occur. The increase in CID efficiency for angiotensin I over methionine enkephalin is due to the effects of multiple charging on ion counting [54]. Multiply charged precursor ions can fragment into two or more product ions, whereas singly charged ions fragment into an ion and a neutral, causing an increase in measured signal and thus apparent collection efficiency.

Peptide Mixture

Resonance excitation was performed on an equimolar mixture of angiotensin I, neurotensin, substance P, and melittin to illustrate the utility of the method for fragmentation of a mixture of mobility-resolved peptides (Figure 5). The primary RF was set such that the smallest precursor, angiotensin I $[M + 3H]^{3+}$, was at $q_{x,y} = 0.707$ (1.35 MHz, 895 V_{p-p}) for the best fragmentation. The primary RF was not changed throughout the experiment. The CID waveform used for the experiment was designed by calculating the secular frequencies for each peptide ion (angiotensin I $[M + 3H]^{3+}$, *m/z* 432.9; neurotensin $[M + 3H]^{3+}$, *m/z* 558.3; substance P $[M + 2H]^{2+}$, *m/z* 674.3; melittin $[M + 4H]^{4+}$, *m/z* 712.14) by Equation 1 applied over the measured drift time for each of the precursors (Figure 5(a)). Excitation amplitudes were experimentally determined to observe the greatest number of fragments for each of the peptides (Table 2). Extensive fragmentation occurs across the range of precursor mobilities (Figure 5(b)). The results of the dipolar excitation experiment are compared to beam-type CID in Figure 5(c). Beam-type CID was performed by raising the bias of the short quadrupole exit orifice as well as the preceding elements to create a 30 V acceleration potential into the collision cell. With beam-type CID, neurotensin shows extensive fragmentation similar to with dipolar excitation. However, the amplitude necessary for fragmentation causes over-fragmentation of angiotensin I to the extent that the precursor and product ions are no longer observed. With acceleration potentials lower than 30V, no

fragmentation was observed. This illustrates the utility of resonantly exciting specific *m/z*'s with different excitation amplitudes in contrast to broadband application of uniform excitation amplitude. Another observation is of low mass fragments not present with beam-type CID. This is evidence that the low mass cutoff of the collision quadrupole affects the observed fragment ion spectra in the beam-type vs. resonant excitation CID.

The product ion mass spectrum for neurotensin is extracted from Figure 5(b) and displayed in Figure 6 to exemplify *de novo* sequencing of peptides by multiplexed IMS/dipolar excitation CID. Peaks that did not match the arrival time distribution of the neurotensin 3^+ precursor or that had inappropriately high charge states (e.g. 3^+ greater than *m/z* 558) were removed during data processing to isolate only neurotensin and its fragments. The product ion spectrum shows mainly y-type fragments due to the increased basicity of the C-terminal portion of the peptide from the arginine residues. 50% sequence coverage is attained, comparable to the results for angiotensin I. Low mass immonium ions (viz. P, I/L, Y) are observed, showing that activation at high $q_{x,y}$ values does not cause loss via low mass cutoff.

Conclusions

A method for multiplexed IMS/CID/MS has been demonstrated by implementing dipolar resonant excitation in a quadrupolar collision cell at ~80 mTorr. CID efficiencies of 44% for singly charged ions have been demonstrated by using an increased Mathieu $q_{x,y}$ stability parameter to allow for faster deposition of internal energy without ion losses. The axial velocity of the ions through the system allows for excitation to occur in a short collision cell after which fragmentation can occur, yielding fragment ions over a broad *m/z* range. This phenomenon is analogous to pulsed-q dissociation or HASTE performed in a beam instrument instead of an ion trap. Efficiencies of up to 84% were observed for multiply charged ions. Reductions in CID efficiency were due to a reduction in fragmentation efficiency with lower AC amplitudes and a reduction in collection efficiency with higher AC amplitudes. Reductions in collection efficiency may be indicative of ion loss due resonant ejection of precursor ions. Finally, the ability to apply resonant excitation in drift time resolved windows was demonstrated with a mixture of peptides. The method performed favorably in comparison with single energy beam-type CID, owing to the ability to tune excitation conditions for each *m/z*. This allowed for extensive fragmentation to be observed for the entire *m/z* range without losing the lower *m/z* peptides. IMS multiplexed resonant excitation CID provides for the ability to obtain extended sequence coverage over a range of *m/z* for peptides in a mobility-resolved complex mixture.

Supplementary Material

Refer to Web version on PubMed Central for supplementary material.

Acknowledgments

Portions of this research were supported by the U.S. Department of Energy (DOE) Office of Biological and Environmental Research Genome Sciences Program under the Pan-omics project, and the NIH National Institute of General Medical Sciences (GM103493 and GM103497). This work was performed in the Environmental Molecular

Science Laboratory (EMSL), a DOE national scientific user facility at the Pacific Northwest National Laboratory (PNNL). PNNL is operated by Battelle for the DOE under contract DE-AC05-76RL0 1830.

References

1. Sleno L, Volmer DA. Ion activation methods for tandem mass spectrometry. J. Mass Spectrom. 2004; 39:1091–1112. [PubMed: 15481084]
2. McLuckey SA. Principles of Collisional Activation in Analytical Mass-Spectrometry. J. Am. Soc. Mass Spectrom. 1992; 3:599–614. [PubMed: 24234564]
3. Beynon JH, Cooks RG, Amy JW, Baitinge We, Ridley TY. Design and Performance of a Mass Analyzed Ion Kinetic-Energy (Mike) Spectrometer. Anal. Chem. 1973; 45 1023-&.
4. Yost RA, Enke CG. Selected Ion Fragmentation with a Tandem Quadrupole Mass-Spectrometer. J. Am. Chem. Soc. 1978; 100:2274–2275.
5. Louris JN, Brodbeltlustig JS, Cooks RG, Glish GL, Vanberkel GJ, Mcluckey SA. Ion Isolation and Sequential Stages of Mass-Spectrometry in a Quadrupole Ion Trap Mass-Spectrometer. Int. J. Mass Spectrom. 1990; 96:117–137.
6. Morris HR, Paxton T, Dell A, Langhorne J, Berg M, Bordoli RS, Hoyes J, Bateman RH. High sensitivity collisionally-activated decomposition tandem mass spectrometry on a novel quadrupole/orthogonal-acceleration time-of-flight mass spectrometer. Rapid Commun. Mass Spectrom. 1996; 10:889–896. [PubMed: 8777321]
7. Vestal ML, Campbell JM. Tandem time-of-flight mass spectrometry. Biol. Mass Spectrom. 2005; 402:79–108.
8. Gauthier JW, Trautman TR, Jacobson DB. Sustained Off-Resonance Irradiation for Collision-Activated Dissociation Involving Fourier-Transform Mass-Spectrometry - Collision-Activated Dissociation Technique That Emulates Infrared Multiphoton Dissociation. Anal. Chim. Acta. 1991; 246:211–225.
9. Goeringer DE, Viehland LA, Danailov DM. Prediction of collective characteristics for ion ensembles in quadrupole ion traps without trajectory simulations. J. Am. Soc. Mass Spectrom. 2006; 17:889–902. [PubMed: 16731002]
10. Tolmachev AV, Vilkov AN, Bogdanov B, Pasa-Tolic L, Masselon CD, Smith RD. Collisional activation of ions in RF ion traps and ion guides: The effective ion temperature treatment. J. Am. Soc. Mass Spectrom. 2004; 15:1616–1628. [PubMed: 15519229]
11. Prentice BM, Santini RE, McLuckey SA. Adaptation of a 3-D Quadrupole Ion Trap for Dipolar DC Collisional Activation. J. Am. Soc. Mass Spectrom. 2011; 22:1486–1492. [PubMed: 21953251]
12. Webb IK, Londry FA, McLuckey SA. Implementation of dipolar direct current (DDC) collision-induced dissociation in storage and transmission modes on a quadrupole/time-of-flight tandem mass spectrometer. Rapid Commun. Mass Spectrom. 2011; 25:2500–2510. [PubMed: 21818811]
13. Paradisi C, Todd JFJ, Traldi P, Vettori U. Boundary Effects and Collisional Activation in a Quadrupole Ion Trap. Org. Mass Spectrom. 1992; 27:251–254.
14. Lammert SA, Cooks RG. Pulsed Axial Activation in the Ion Trap - a New Method for Performing Tandem Mass-Spectroscopy (MS/MS). Rapid Commun. Mass Spectrom. 1992; 6:528–530.
15. Wang MD, Schachterle S, Wells G. Application of nonresonance excitation to ion trap tandem mass spectrometry and selected ejection chemical ionization. J. Am. Soc. Mass Spectrom. 1996; 7:668–676. [PubMed: 24203482]
16. Louris JN, Cooks RG, Syka JEP, Kelley PE, Stafford GC, Todd JFJ. Instrumentation, Applications, and Energy Deposition in Quadrupole Ion-Trap Tandem Mass-Spectrometry. Anal. Chem. 1987; 59:1677–1685.
17. March RE. An introduction to quadrupole ion trap mass spectrometry. J. Mass Spectrom. 1997; 32:351–369.
18. Fenn JB, Mann M, Meng CK, Wong SF, Whitehouse CM. Electrospray Ionization for Mass-Spectrometry of Large Biomolecules. Science. 1989; 246:64–71. [PubMed: 2675315]
19. Karas M, Bachmann D, Bahr U, Hillenkamp F. Matrix-Assisted Ultraviolet-Laser Desorption of Nonvolatile Compounds. Int. J. Mass Spectrom. 1987; 78:53–68.

20. Aebersold R, Mann M. Mass spectrometry-based proteomics. Nature. 2003; 422:198–207. [PubMed: 12634793]
21. Yates JR, Ruse CI, Nakorchevsky A. Proteomics by Mass Spectrometry: Approaches, Advances, and Applications. Annu. Rev. Biomed. Eng. 2009; 11:49–79. [PubMed: 19400705]
22. Wilm M, Neubauer G, Mann M. Parent ion scans of unseparated peptide mixtures. Anal. Chem. 1996; 68:527–533. [PubMed: 8712361]
23. Williams JD, Flanagan M, Lopez L, Fischer S, Miller LAD. Using accurate mass electrospray ionization-time-of-flight mass spectrometry with in-source collision-induced dissociation to sequence peptide mixtures. J. Chromatogr. A. 2003; 1020:11–26. [PubMed: 14661753]
24. Masselon C, Anderson GA, Harkewicz R, Bruce JE, Pasa-Tolic L, Smith RD. Accurate mass multiplexed tandem mass spectrometry for high-throughput polypeptide identification from mixtures. Anal. Chem. 2000; 72:1918–1924. [PubMed: 10784162]
25. Chakraborty AB, Berger SJ, Gebler JC. Use of an integrated MS-multiplexed MS/MS data acquisition strategy for high-coverage peptide mapping studies. Rapid Commun. Mass Spectrom. 2007; 21:730–744. [PubMed: 17279597]
26. Gillet LC, Navarro P, Tate S, Rost H, Selevsek N, Reiter L, Bonner R, Aebersold R. Targeted Data Extraction of the MS/MS Spectra Generated by Data-independent Acquisition: A New Concept for Consistent and Accurate Proteome Analysis. Mol. Cell. Proteomics. 2012; 11
27. Li L, Masselon CD, Anderson GA, Pasa-Tolic L, Lee SW, Shen Y, Zhao R, Lipton MS, Conrads TP, Tolic N, Smith RD. High-throughput peptide identification from protein digests using data-dependent multiplexed tandem FTICR mass spectrometry coupled with capillary liquid chromatography. Anal. Chem. 2001; 73:3312–3322. [PubMed: 11476231]
28. Haller I, Mirza UA, Chait BT. Collision induced decomposition of peptides. Choice of collision parameters. J. Am. Soc. Mass Spectrom. 1996; 7:677–681. [PubMed: 24203483]
29. Bohrer BC, Mererbloom SI, Koeniger SL, Hilderbrand AE, Clemmer DE. Biomolecule Analysis by Ion Mobility Spectrometry. Annu.Rev. Anal. Chem. 2008; 1:293–327.
30. Fenn LS, McLean JA. Biomolecular structural separations by ion mobility-mass spectrometry. Anal. Bioanal. Chem. 2008; 391:905–909. [PubMed: 18320175]
31. Kanu AB, Dwivedi P, Tam M, Matz L, Hill HH. Ion mobility-mass spectrometry. J. Mass Spectrom. 2008; 43:1–22. [PubMed: 18200615]
32. Zolotov YA. Ion mobility spectrometry. J. Anal. Chem. 2006; 61:519–519.
33. Tang K, Shvartsburg AA, Lee HN, Prior DC, Buschbach MA, Li F, Tolmachev AV, Anderson GA, Smith RD. High-sensitivity ion mobility spectrometry/mass spectrometry using electrodynamic ion funnel interfaces. Anal. Chem. 2005; 77:3330–3339. [PubMed: 15889926]
34. Baker ES, Clowers BH, Li F, Tang K, Tolmachev AV, Prior DC, Belov ME, Smith RD. Ion mobility spectrometry-mass spectrometry performance using electrodynamic ion funnels and elevated drift gas pressures. J. Am. Soc. Mass Spectrom. 2007; 18:1176–1187. [PubMed: 17512752]
35. Valentine SJ, Counterman AE, Hoaglund CS, Reilly JP, Clemmer DE. Gas-phase separations of protease digests. J. Am. Soc. Mass Spectrom. 1998; 9:1213–1216. [PubMed: 9794086]
36. Hoaglund-Hyzer CS, Clemmer DE. Ion trap/ion mobility/quadrupole/time of flight mass spectrometry for peptide mixture analysis. Anal. Chem. 2001; 73:177–184. [PubMed: 11199963]
37. Lee YJ, Hoaglund-Hyzera CS, Barnes CAS, Hilderbrand AE, Valentine SJ, Clemmer DE. Development of high-throughput liquid chromatography injected ion mobility quadrupole time-of-flight techniques for analysis of complex peptide mixtures. J. Chromatogr., B: Anal. Technol. Biomed. Life Sci. 2002; 782:343–351.
38. Ruotolo BT, Gillig KJ, Stone EG, Russell DH. Peak capacity of ion mobility mass spectrometry: Separation of peptides in helium buffer gas. J. Chromatogr., B: Anal. Technol. Biomed. Life Sci. 2002; 782:385–392.
39. Crowell KL, Baker ES, Payne SH, Ibrahim YI, Monroe ME, Slysz GW, LaMarche BL, Petyuk VA, Piehowski PD, Danielson WFI, Anderson GA, Smith RD. Increasing confidence of LC–MS identifications by utilizing ion mobility spectrometry. Int. J. Mass Spectrom. 2013 http://dx.doi.org/10.1016/j.ijms.2013.06.028.

40. Hoadlund-Hyzer CS, Li JW, Clemmer DE. Mobility labeling for parallel CID of ion mixtures. Anal. Chem. 2000; 72:2737–2740. [PubMed: 10905301]
41. Koeniger SL, Valentine SJ, Myung S, Plasencia M, Lee YJ, Clemmer DE. Development of field modulation in a split-field drift tube for high-throughput multidimensional separations. J. Proteome Res. 2005; 4:25–35. [PubMed: 15707354]
42. Baker ES, Tang KQ, Danielson WF, Prior DC, Smith RD. Simultaneous fragmentation of multiple ions using IMS drift time dependent collision energies. J. Am. Soc. Mass Spectrom. 2008; 19:411–419. [PubMed: 18226544]
43. Ibrahim YM, Prior DC, Baker ES, Smith RD, Belov ME. Characterization of an ion mobility-multiplexed collision-induced dissociation-tandem time-of-flight mass spectrometry approach. Int. J. Mass Spectrom. 2010; 293:34–44. [PubMed: 20596241]
44. Belov ME, Gorshkov MV, Udseth HR, Anderson GA, Tolmachev AV, Prior DC, Harkewicz R, Smith RD. Initial implementation of an electrodynamic ion funnel with Fourier transform ion cyclotron resonance mass spectrometry. J. Am. Soc. Mass Spectrom. 2000; 11:19–23. [PubMed: 10631660]
45. Shaffer SA, Prior DC, Anderson GA, Udseth HR, Smith RD. An ion funnel interface for improved ion focusing and sensitivity using electrospray ionization mass spectrometry. Anal. Chem. 1998; 70:4111–4119. [PubMed: 9784749]
46. Shaffer SA, Tolmachev A, Prior DC, Anderson GA, Udseth HR, Smith RD. Characterization of an improved electrodynamic ion funnel interface for electrospray ionization mass spectrometry. Anal. Chem. 1999; 71:2957–2964. [PubMed: 10450147]
47. Clowers BH, Ibrahim YM, Prior DC, Danielson WF 3rd, Belov ME, Smith RD. Enhanced ion utilization efficiency using an electrodynamic ion funnel trap as an injection mechanism for ion mobility spectrometry. Anal. Chem. 2008; 80:612–623. [PubMed: 18166021]
48. Ibrahim Y, Belov ME, Tolmachev AV, Prior DC, Smith RD. Ion funnel trap interface for orthogonal time-of-flight mass spectrometry. Anal. Chem. 2007; 79:7845–7852. [PubMed: 17850113]
49. Sztaray J, Memboeuf A, Drahos L, Vekey K. Leucine Enkephalin-a Mass Spectrometry Standard. Mass Spectrom. Rev. 2011; 30:298–320. [PubMed: 20669325]
50. Murrell J, Despeyroux D, Lammert SA, Stephenson JL, Goeringer DE. "Fast excitation" CID in a quadrupole ion trap mass spectrometer. J. Am. Soc. Mass Spectrom. 2003; 14:785–789. [PubMed: 12837601]
51. Cunningham C, Glish GL, Burinsky DJ. High amplitude short time excitation: A method to form and detect low mass product ions in a quadrupole ion trap mass spectrometer. J. Am. Soc. Mass Spectrom. 2006; 17:81–84. [PubMed: 16352436]
52. Schwartz, JC.; Syka, JEP.; Quarmby, ST. 53rd ASMS Conference on Mass Spectrometry and Allied Topics; San Antonio, TX. 2005.
53. Yost RA, Enke CG, Mcgilvery DC, Smith D, Morrison JD. High-Efficiency Collision-Induced Dissociation in an Rf-Only Quadrupole. Int. J. Mass Spectrom. 1979; 30:127–136.
54. Thomson BA, Douglas DJ, Corr JJ, Hager JW, Jolliffe CL. Improved Collisionally Activated Dissociation Efficiency and Mass Resolution on a Triple Quadrupole Mass-Spectrometer System. Anal. Chem. 1995; 67:1696–1704.
55. Schwartz BL, Bursey MM. Some Proline Substituent Effects in the Tandem Mass-Spectrum of Protonated Pentaalanine. Biol. Mass Spectrom. 1992; 21:92–96. [PubMed: 1606186]
56. Harrison AG. The gas-phase basicities and proton affinities of amino acids and peptides. Mass Spectrom. Rev. 1997; 16:201–217.
57. Bleiholder C, Suhai S, Paizs B. Revising the proton affinity scale of the naturally occurring alpha-amino acids. J. Am. Soc. Mass Spectrom. 2006; 17:1275–1281. [PubMed: 16829127]
58. Vaisar T, Urban J. Probing the proline effect in CID of protonated peptides. J. Mass Spectrom. 1996; 31:1185–1187. [PubMed: 8916427]
59. Knapp-Mohammady M, Young AB, Paizs B, Harrison AG. Fragmentation of Doubly-Protonated Pro-His-Xaa Tripeptides: Formation of b(2)(2+) Ions. J. Am. Soc. Mass Spectrom. 2009; 20:2135–2143. [PubMed: 19683937]

60. Breci LA, Tabb DL, Yates JR, Wysocki VH. Cleavage N-terminal to proline: Analysis of a database of peptide tandem mass spectra. Anal. Chem. 2003; 75:1963–1971. [PubMed: 12720328]

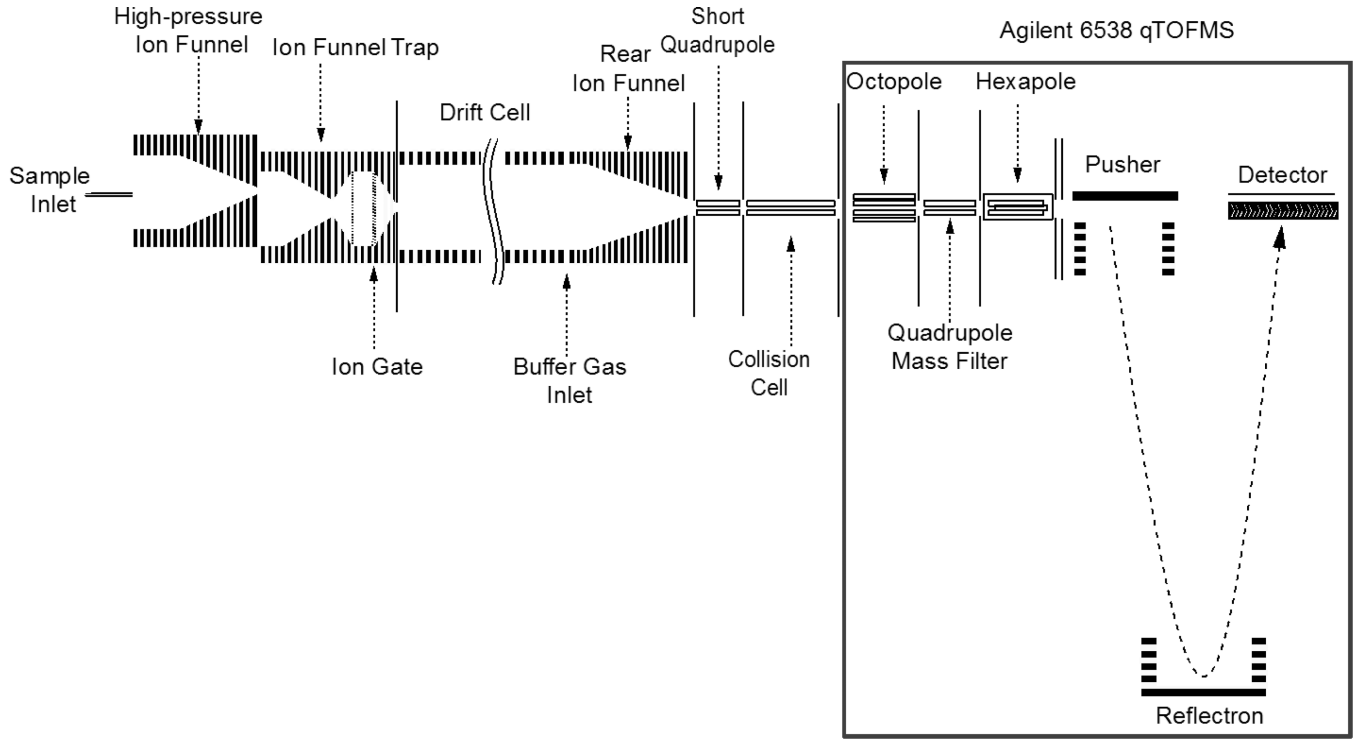

Figure 1.
Illustration of the IMS/qTOF MS instrument used in this work.

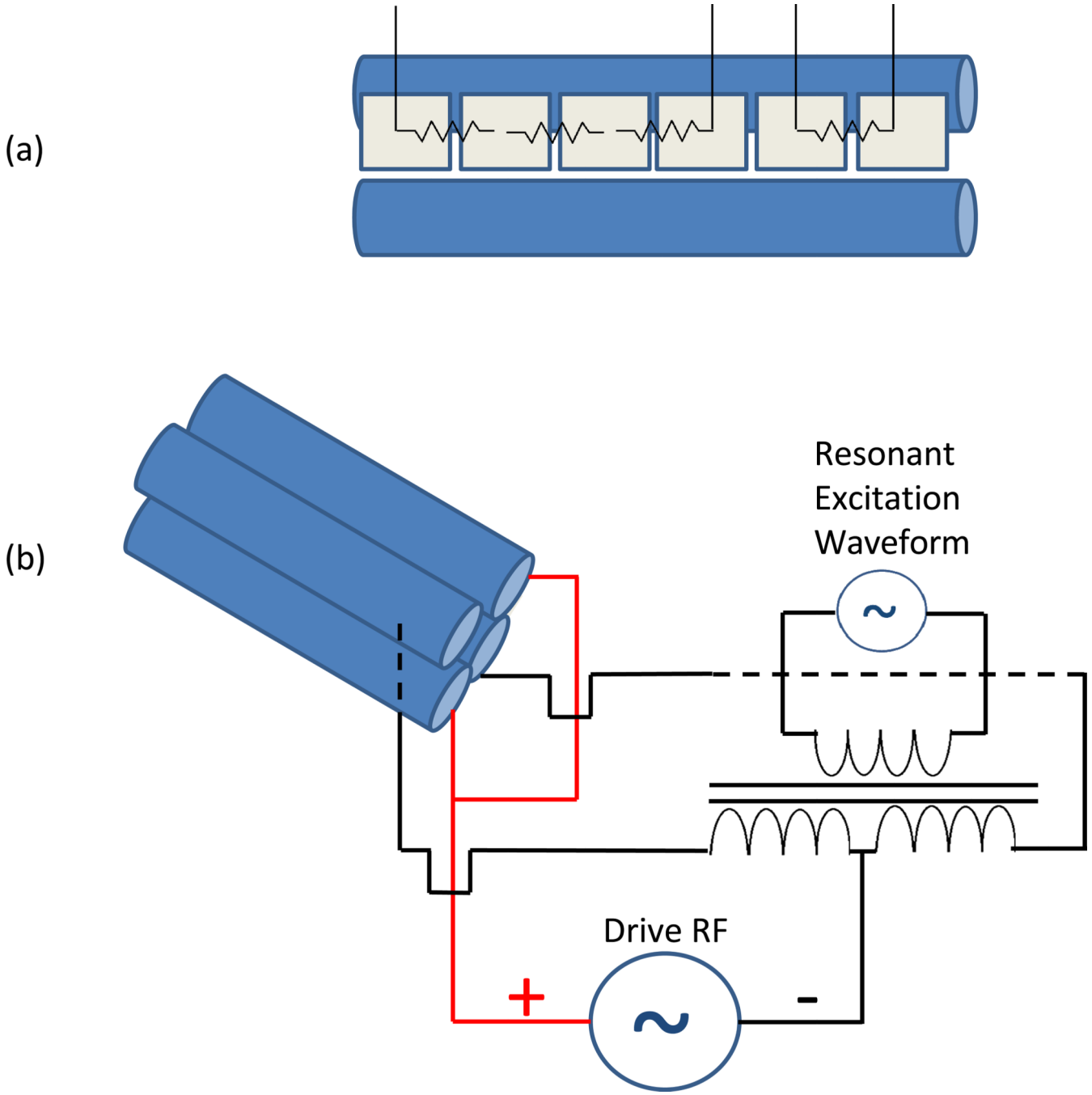

Figure 2.
(a) Illustration showing a single segmented vane divided into two resistively coupled sections, and (b) approach used for the superposition of dipolar AC onto the drive RF for resonant excitation.

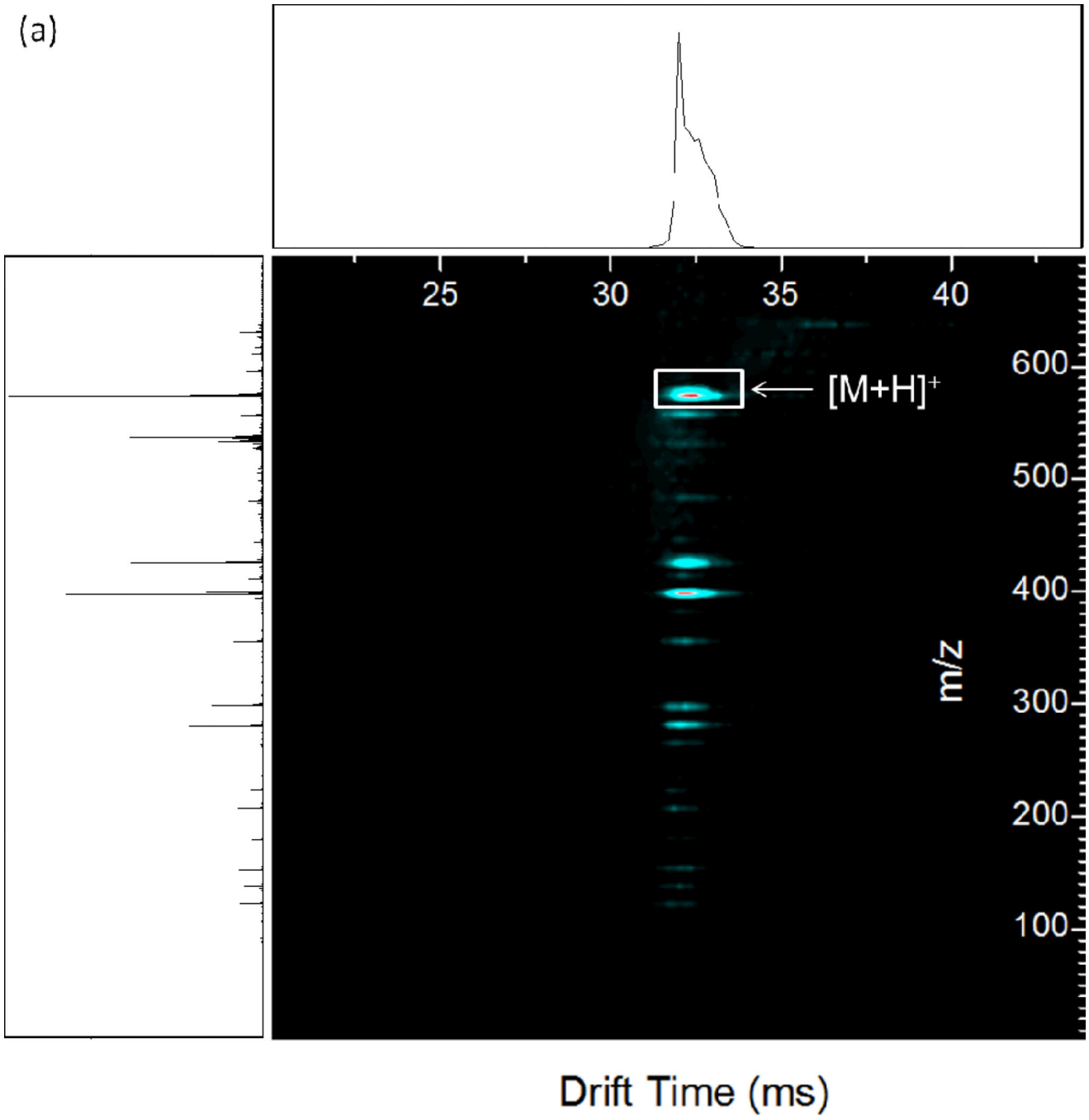

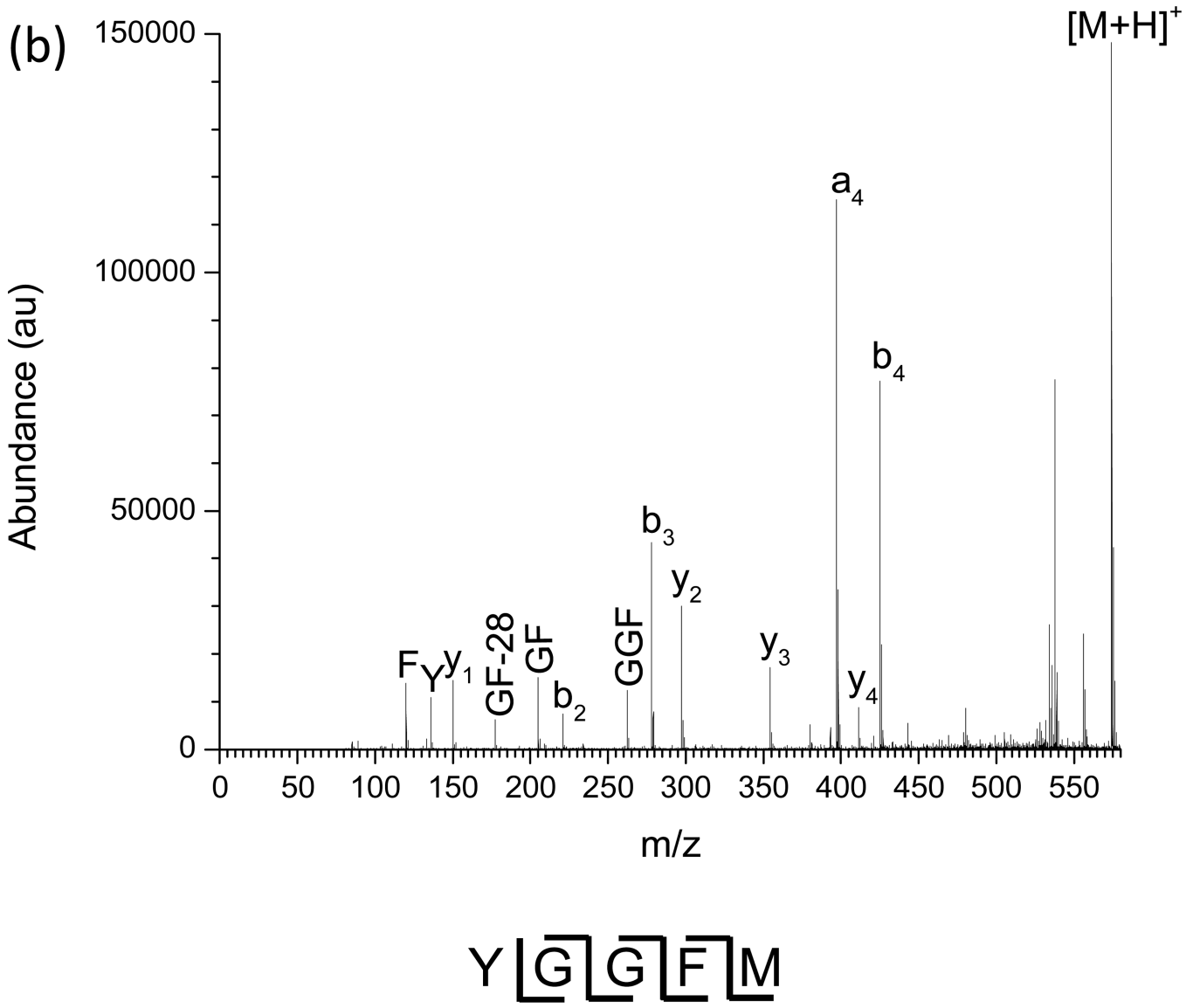

Figure 3.

(a) Nested IMS/MS product ion spectrum of methionine enkephalin. 1.35 MHz, 1188 $V_{p\text{-}p}$ main RF; 338 kHz, 4.0 $V_{p\text{-}p}$ applied resonant excitation waveform, applied from time 29–34 ms. (b) Mass spectrum under the same conditions as (a). Known fragment ions are labeled.

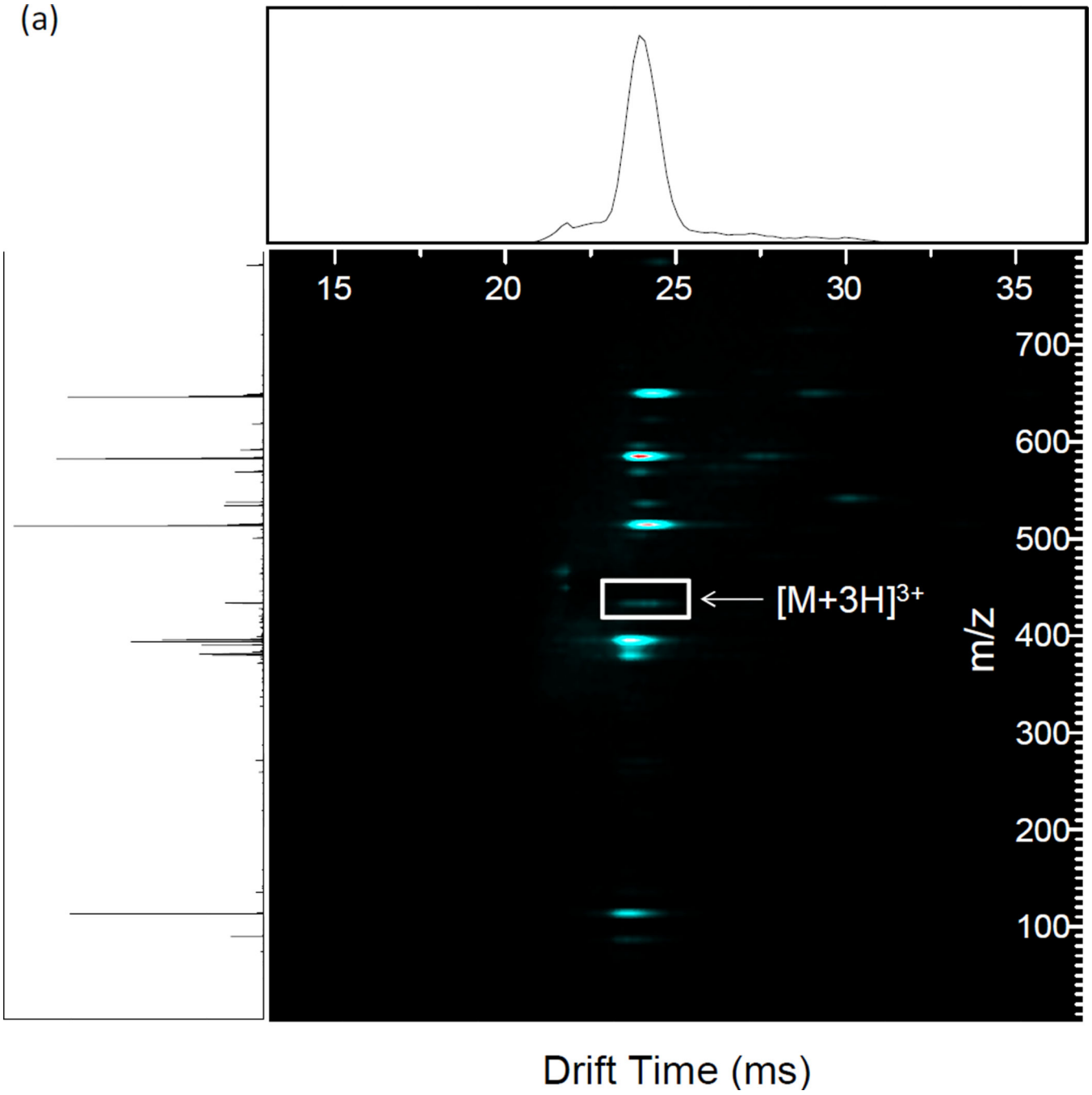

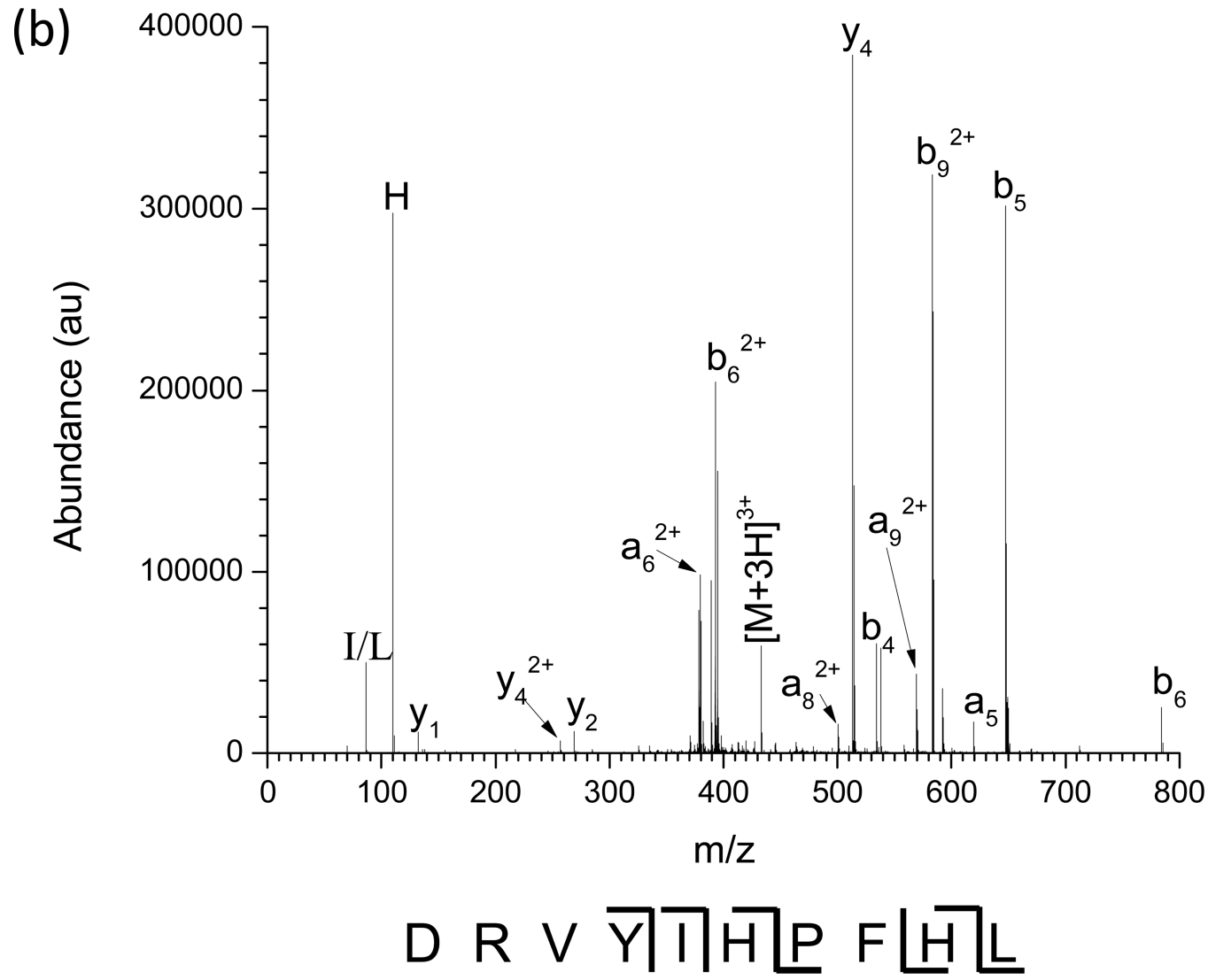

Figure 4.

(a) Nested IMS/MS product ion spectrum of angiotensin I 3^{+}. 1.35 MHz, 890 $V_{p\text{-}p}$ main RF; 336 kHz, 8.8 $V_{p\text{-}p}$ applied resonant excitation waveform, applied from time 21–26 ms. (b) Mass spectrum under the same conditions as (a). Known fragment ions are labeled.

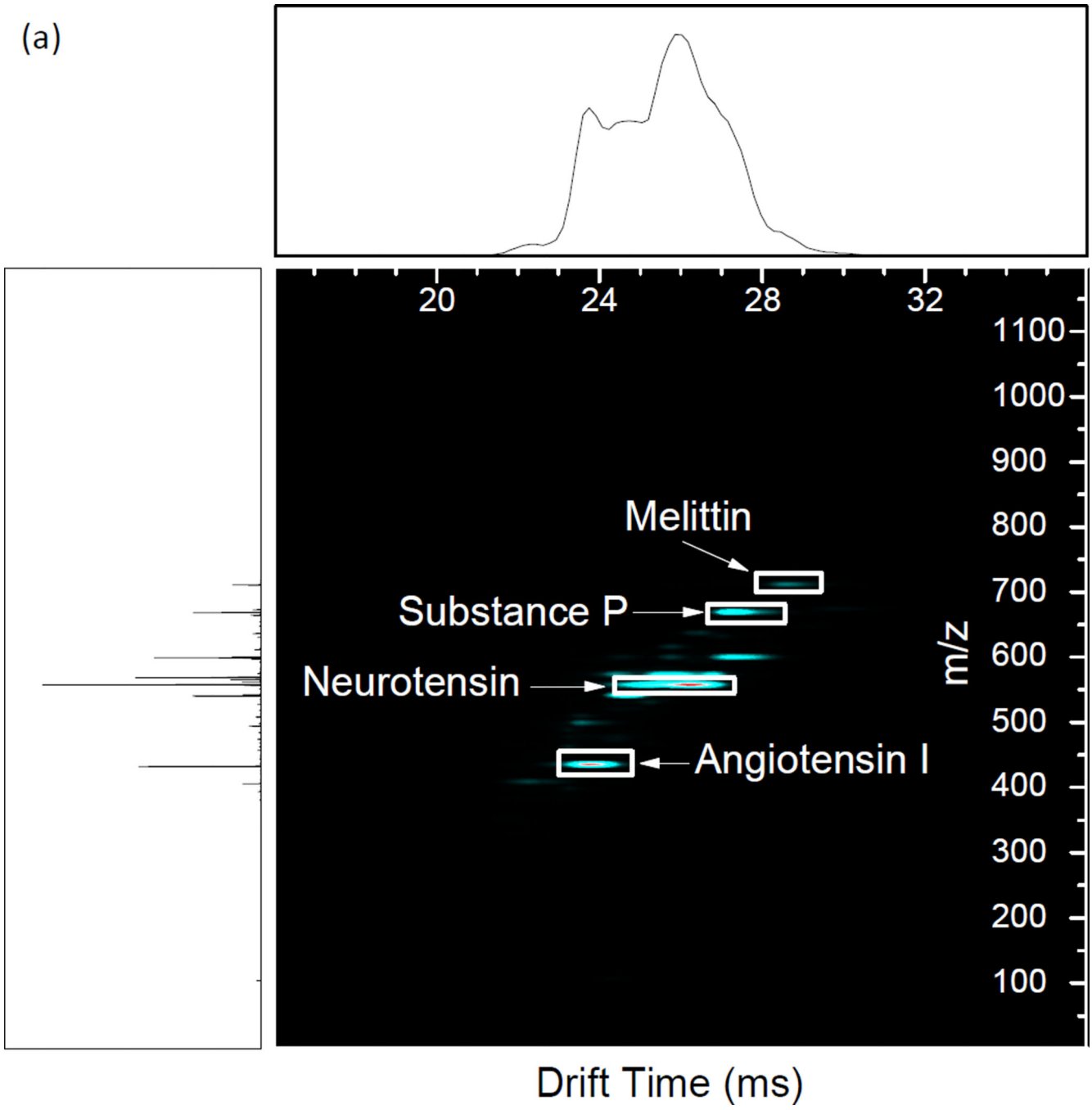

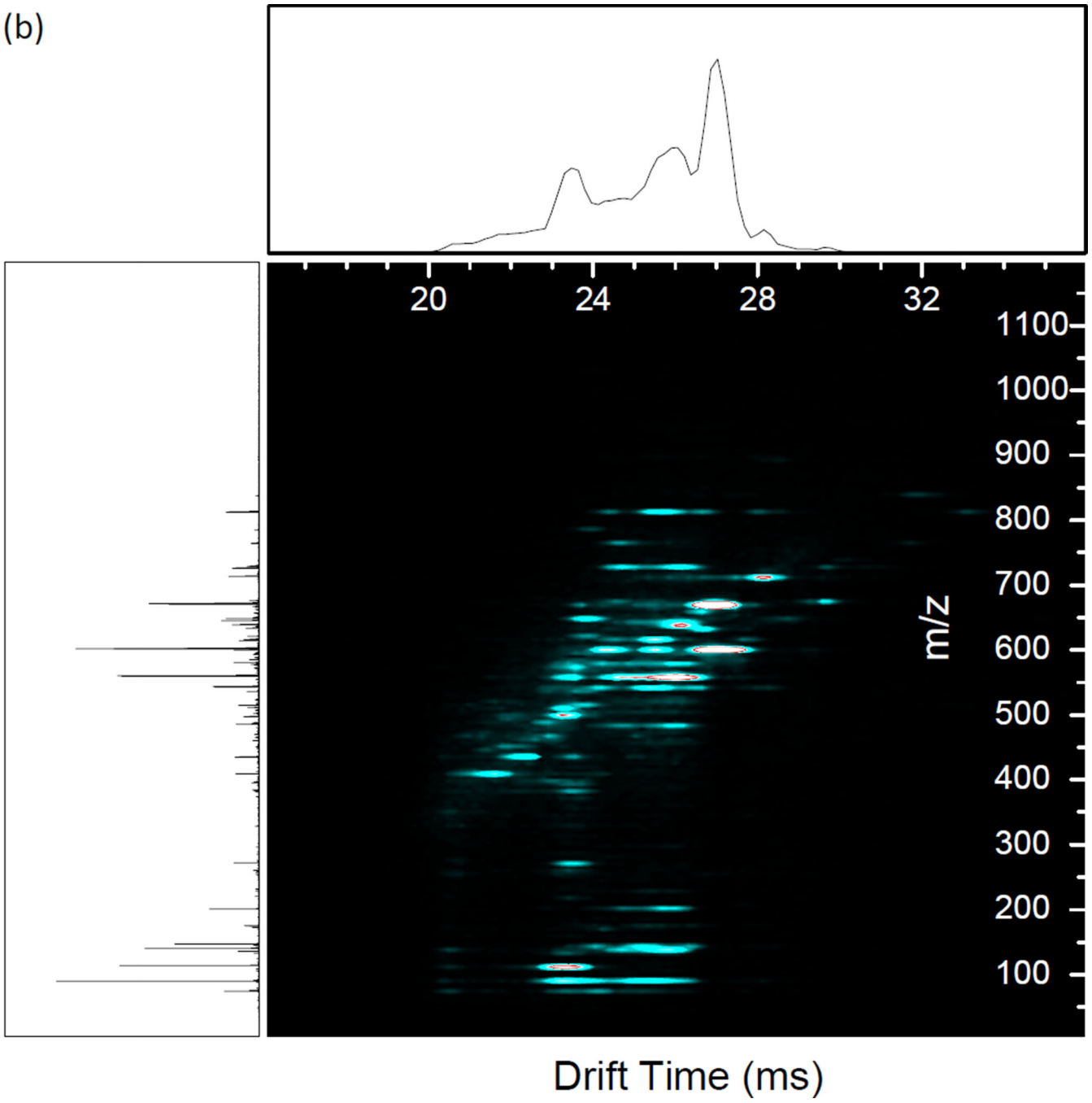

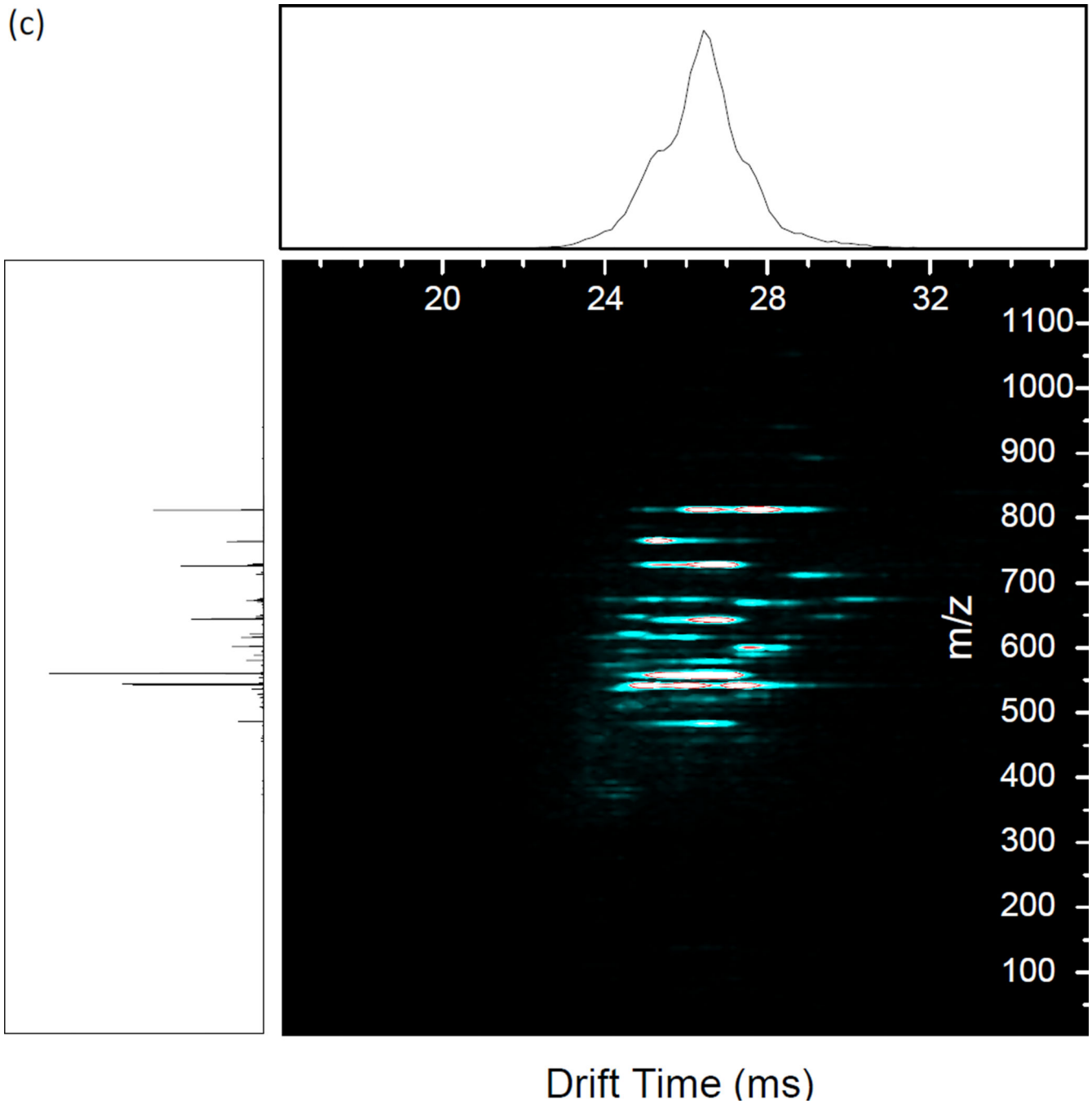

Figure 5.

(a) Precursor IMS/MS spectrum of the 4 peptide mixture. Precursor identities are labeled. (b) Resonance excitation CID of the 4 peptide mixture using the waveform detailed in Table 2. (c) Single energy beam-type CID of the 4 peptide mixture. CID was performed by creating a 30 V potential between the conductance limiting orifice after the short quadrupole and the input voltage of the first segment of the vane in the collision cell. Main RF was 1.35 MHz, 895 V_{p-p} for all experiments.

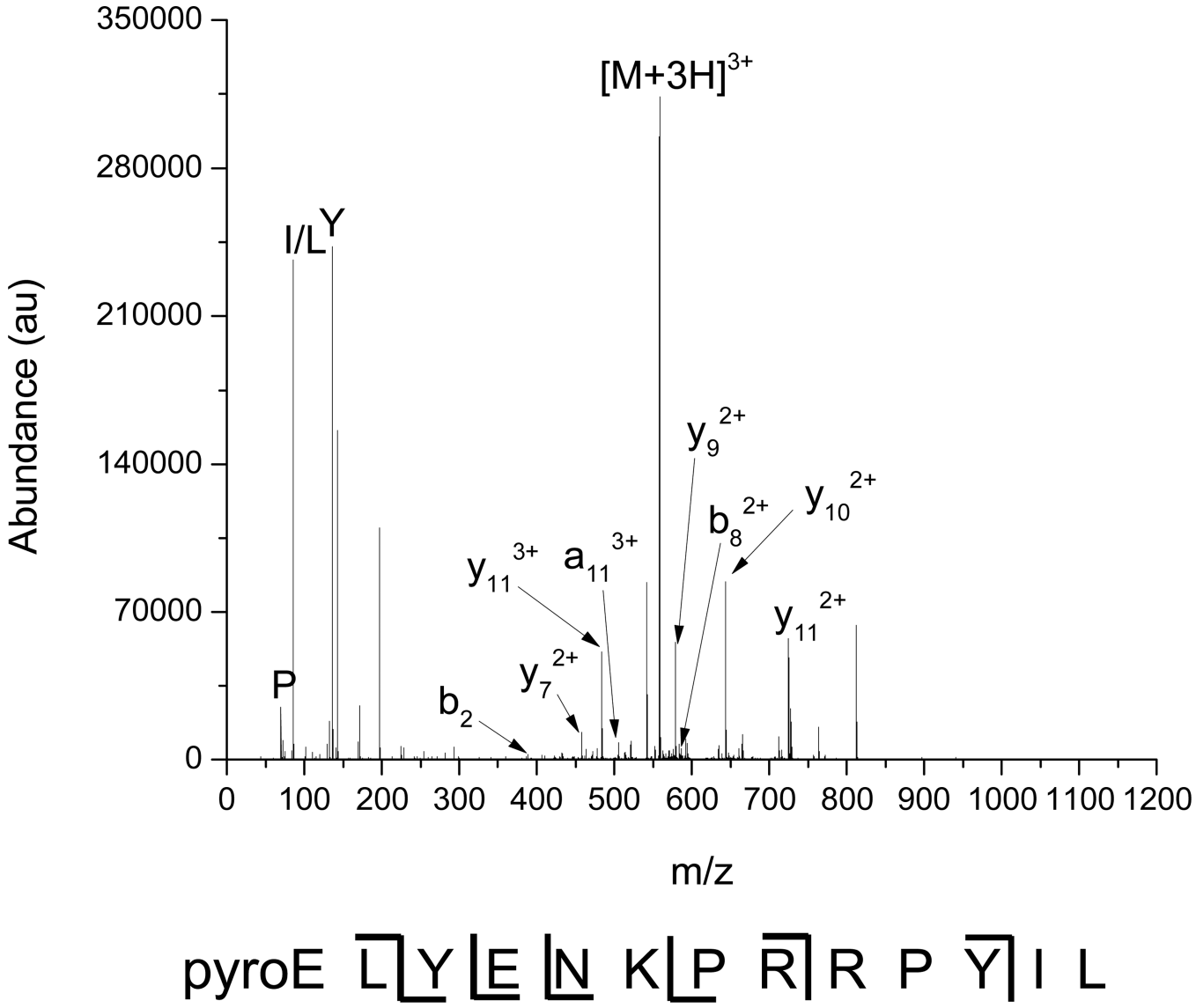

Figure 6.

Extracted mass spectrum for neurotensin 3^{+} and its fragments. Ions with unaligned drift times and inappropriately high charge states have been removed.

Table 1

Tabulated fragmentation, collection, and CID efficiencies for resonant excitation CID under various amplitudes for (a) methionine enkephalin at 338 kHz and (b) angiotensin I 3^+ at 336 kHz.

(a)	4.8V	5.6V	6.4V	7.2V	8V	8.8V	9.6V
E_f	.16	.25	.37	.57	.65	.73	.52
E_c	.93	.85	.78	.77	.50	.32	.09
E_{CID}	.15	.21	.29	.44	.33	.24	.05

(b)	4.8V	5.6V	6.4V	6.72V	7.2V	7.68V	8V	8.32V	8.8V	9.6V	10.4V
E_f	0	0	.10	.17	.34	.56	.81	.95	1.00	1.00	1.00
E_c	.91	.88	.93	.93	.92	.94	.99	.88	.76	.68	.65
E_{CID}	0	0	.9	.16	.31	.53	.80	.84	.76	.68	.65

J Am Soc Mass Spectrom. Author manuscript; available in PMC 2014 July 28.

Table 2

Resonant excitation waveform for 4 peptide mix, representing a sum of sine waves. Main RF: 1.35 MHz, 895 $V_{p\text{-}p}$.

Peptide	Amplitude, $V_{p\text{-}p}$	Frequency, kHz	Time, ms
Angiotensin I, 3^+	8	337	21.8 – 24
Neurotensin, 3^+	11.2 – 12	262	22.8 – 27
Substance P, 2^+	4.8	217	27.3 – 30
Melittin, 4^+	11.2	205	26.5 – 28.5